Using observational and reanalysis data to explore the Gulf of California boundary layer during the North American Monsoon onset

Mariam Fonseca-Hernandez[1], Cuauhtémoc Turrent[2], Yandy Gonzalez-Mayor[1], and Irina Tereshchenko[3]

[1]Centro de Investigación Científica y de Educación Superior de Ensenada
[2]CICESE
[3]Universidad de Guadalajara

November 21, 2022

Abstract

This paper uses rawinsondes and pilot balloon data from the 2004 North American Monsoon (NAM) Experiment, as well as satellite-based products and reanalysis datasets that span 1982 to 2018, to analyze the mixing mechanisms responsible for the temporal and spatial variations of the Gulf of California (GoC) boundary layer during the NAM onset. We show that the regional diurnal cycle is strongly affected by low-level convergence and divergence associated with local breeze regimes and by the presence and intensity of a thermal inversion over the gulf. Earlier starting monsoons have less moisture available for precipitation than those starting later in the calendar year. Therefore, early onset monsoons have less rainfall during their first month, which is a result that is in contrast with previous studies that have analyzed the timing of the NAM but only reported seasonal precipitation totals. The GoC boundary layer height at the time of monsoon onset, found to be controlled by the gulf's surface temperature, has a significant impact on the precipitation over Sonora, Sinaloa, and southern Arizona. After the erosion of the thermal inversion over the GoC that coincides with the NAM onset, wind shear produced by the region's unique geographic and topographic features is the largest source of turbulence for the mixing of the boundary layer. Hence, our results suggest that a numerical model used to forecast or analyze NAM precipitation must have enough spatial resolution to adequately reproduce the effects that the GoC's features have on its complex diurnal circulation systems.

Using observational and reanalysis data to explore the Gulf of California boundary layer during the North American Monsoon onset

Mariam Fonseca-Hernandez[1], Cuauhtémoc Turrent[1], Yandy G. Mayor[1] and Iryna Tereshchenko[2]

[1]Department of Physical Oceanography, CICESE, Ensenada, Baja California, Mexico.

[2]Physics Department, University of Guadalajara, Guadalajara, Jalisco, Mexico.

Corresponding author: Mariam Fonseca-Hernandez (mfonseca@cicese.edu.mx)

Key Points:

- Earlier starting monsoons are associated with drier starts and late onsets to wetter starts.
- Monsoon precipitation over Sonora, Sinaloa, and southern Arizona is closely related to variations of the Gulf of California boundary layer.
- After monsoon onset, wind shear is the largest source of turbulence for the mixing of the Gulf of California boundary layer.

Abstract

This paper uses rawinsondes and pilot balloon data from the 2004 North American Monsoon (NAM) Experiment, as well as satellite-based products and reanalysis datasets that span 1982 to 2018, to analyze the mixing mechanisms responsible for the temporal and spatial variations of the Gulf of California (GoC) boundary layer during the NAM onset. We show that the regional diurnal cycle is strongly affected by low-level convergence and divergence associated with local breeze regimes and by the presence and intensity of a thermal inversion over the gulf. Earlier starting monsoons have less moisture available for precipitation than those starting later in the calendar year. Therefore, early onset monsoons have less rainfall during their first month, which is a result that is in contrast with previous studies that have analyzed the timing of the NAM but only reported seasonal precipitation totals. The GoC boundary layer height at the time of monsoon onset, found to be controlled by the gulf's surface temperature, has a significant impact on the precipitation over Sonora, Sinaloa, and southern Arizona. After the erosion of the thermal inversion over the GoC that coincides with the NAM onset, wind shear produced by the region's unique geographic and topographic features is the largest source of turbulence for the mixing of the boundary layer. Hence, our results suggest that a numerical model used to forecast or analyze NAM precipitation must have enough spatial resolution to adequately reproduce the effects that the GoC's features have on its complex diurnal circulation systems.

1 Introduction

The North American Monsoon (NAM) moisture sources have been an important scientific question since the phenomenon was first described (Douglas et al., 1993). A review of this issue up until 1997 can be found in Adams and Comrie (1997). Their conclusions regarding moisture sources have been largely supported by later studies, which have confirmed that the Gulf of California (GoC) plays an essential role for the NAM system because the mean low level atmospheric circulation over the gulf is the largest source of moisture for the core region during the monsoon onset (Barron et al., 2012, Dominguez et al., 2016).

In an observational study by Erfani and Mitchell (2014), the presence of a thermal inversion over the GoC before the monsoon onset was documented for the 2004 season using the North American Monsoon Experiment (NAME) dataset. That study suggests a local-scale mechanism in which the thermal inversion controls low-level moisture prior to the onset. Additionally, the diurnal circulation increases the subsidence over the gulf and enhances the strength of the inversion, thus restricting vertical mixing. As a consequence, moisture content increases in the air below the inversion cap. But when the sea surface temperature of the gulf exceeds 29 °C the inversion fades, allowing the trapped moisture to mix with the free tropospheric air and increasing water vapor available for precipitation. Also, Mitchell et al. (2002) found that monsoon rainfall does not occur unless the surface temperature of the gulf exceeds 26°C.

Therefore, not only is the GoC a primary moisture source during the NAM onset, but the structure of its boundary layer also appears to be a key element of the monsoon system. Only a few studies have addressed at any length the GoC boundary layer, most likely because observations of the vertical structure of the atmosphere over the gulf are sparse and insufficient.

Badan-Dangon et al. (1991) is one of the first studies published on the structure of the lower atmosphere (<2 km) over the GoC. They used soundings, meteorological observations, and instrumented flights to introduce a conceptual model for the gulf marine layer, highlighting the differences between winter and summer. The summer marine layer is described to be between 200 and 300 m thick, humid and warm. A dry layer of subsiding air was found directly above, with a thermal inversion of 2-3 °C in between. This study remains perhaps the most comprehensive description of the gulf boundary layer structure to date.

Additional relevant papers using the NAME dataset include Zuidema et al. (2007) and Johnson et al. (2010). The former reported a mean atmospheric boundary layer of about 410 m depth and moist layers located between 2-3 km and 5-6 km of altitude associated with the local land-sea breeze system and with convective outflow from mainland Mexico, respectively. They used observations collected from the Altair Research Vessel near the mouth of the GoC (~23.5 °N, 108 °W), between July 7 and August 11, 2004. The latter study focused on the diurnal cycle of convection, and found that condensation heating and moistening by deep convection are restrained to the lower atmosphere and peak during nighttime. They documented a clear land/sea breeze signal over the western slopes of the Sierra Madre Occidental (SMO), and that convection behaves differently over the gulf.

If Erfani and Mitchell (2014)'s ideas on the role of the GoC boundary layer regarding the monsoon onset are correct, the following questions arise: How does the thermal inversion over the GoC form and how is it sustained before the monsoon onset? Which physical mechanisms control the evolution of the boundary layer? How does the vertical mixing of water vapor that marks the NAM onset occur? We believe that some elements for the answers to these questions, concerning the GoC boundary layer structure and dynamics, can be clarified by further analysis of existing observational data, before turning to numerical simulations. With that purpose in mind, this paper uses measurements collected during the NAME campaign as well as data from satellite and rain-gauge merged precipitation and reanalysis products to describe the spatial structure and temporal evolution of the marine boundary layer over the GoC leading up to and after the NAM onset. In the following section we describe the data and methods and introduce a simple method to determine the boundary layer height using high resolution rawinsonde data. This method is based on the vertical gradients of temperature and relative humidity and is appropriate for very high vertical resolution data. In section three we present noteworthy correlations between the monsoon onset date and the average daily precipitation and between the gulf's boundary layer height and its sea surface temperature. Also, we discuss the mechanisms for the mixing of the GoC's marine layer in the context of the NAM onset and present a spatial correlation analysis between the monsoon precipitation over land and the height of the boundary layer over the gulf.

2 Data and Methods

2.1 Study area

The study area is presented in Fig. 1a and covers most of northwestern Mexico. The orientation axis of the GoC is NNW-SSE, and it extends approximately from 23° to 32 °N with a length of about 1500 km and a mean width of 200 km. The GoC connects to the Pacific Ocean to the south and is surrounded by the Baja California (BC) peninsula and the Mexican states of Sonora and Sinaloa. Fig. 1b shows that the peninsula has terrain elevations below 2 km and several topographic lows that are zonally oriented. On the mainland side, the SMO is a major mountain range system roughly parallel to the GoC axis. The terrain data is taken from the Shuttle Radar Topographic Mission 3 arc second (SRTM-3; Farr et al., 2007).

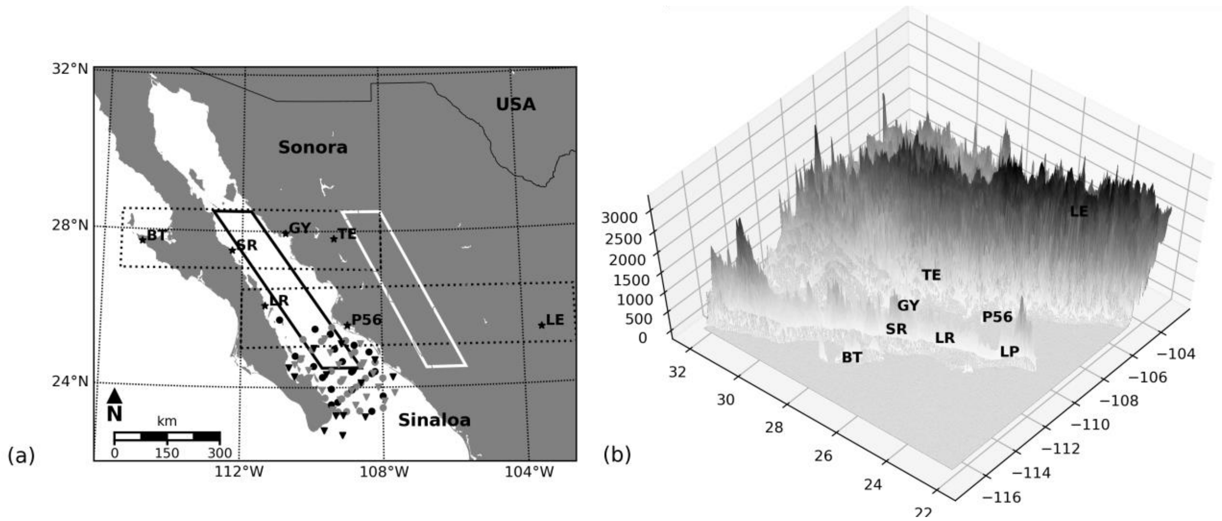

Figure 1. **(a)** Study area. **(b)** Regional topography from the Shuttle Radar Topographic Mission 3 arc second (SRTM-3). Black stars in (a) are the locations of the NAME pilot balloon (PIBAL) measurements: Bahía Tortuga (BT), Santa Rosalía (SR), Empalme (GY), Tesopaco (TE), Loreto (LR), Topolobampo (P56), and Lerdo (LE); gray markers indicate locations of NAME offshore soundings done without wind measurements, while black markers show the locations of the rawinsondes that included wind measurements. Circles show the 2004 June (pre-onset) soundings while triangles mark the 2004 August (post-onset) soundings. The white and black polygons will be used to identify the onset date and to analyze the boundary layer height over the GoC, respectively.

2.2 Observations

We used high vertical resolution (2 seconds) NAME (Higgins et al., 2006) rawinsonde data from the Francisco de Ulloa Research Vessel to study the GoC boundary layer. The rawinsondes were launched during two separate cruises to the GoC: June 5-21 (circles) and August 6-16 2004 (triangles); see Fig. 1a. Soundings were typically released four times per day and measured temperature, pressure and humidity. The green markers in Fig. 1a represent the soundings that also included wind measurements and were more often released at 0400 and 1600 local time (LT); red markers represent soundings done without wind measurements and were more often launched at 1000 and 2200 LT.

We also used wind data as a function of height from NAME pilot balloons (PIBAL). The black dots in Fig. 1a indicate the seven PIBAL stations we considered; see Table 1. The PIBAL sounding sites are almost in latitudinal alignment with the 26° and 28° N parallels. Almost all PIBAL soundings were taken at 0600 and 1600 LT. For our analysis, the 0600 LT PIBAL data is taken as representative of the nocturnal flow while the 1600 LT PIBAL data represents the daytime flow. A NAME PIBAL station was located at 24° N near the city of La Paz, on the west coast of the GoC. However, since no corresponding eastern PIBAL station was set up on the mainland we didn’t include a wind analysis for this latitude.

Table 1. PIBAL station data.

ID	Site	Longitude	Latitude	Elevation (m)	June Launches	August Launches
BT	Bahía Tortugas	-114.90	27.70	18	7	38
SR	Santa Rosalía	-112.29	27.50	33	55	55
GY	Empalme	-100.76	27.95	12	59	57
TE	Tesopaco	-109.35	27.81	440	73	79
LR	Loreto	-111.33	26.10	7	49	40
P56	Topolobampo	-108.98	25.60	12	58	55
LE	Lerdo (Torreón)	-103.46	25.45	1130	9	19

We analyzed the boundary layer height (blh) from four different reanalyses datasets: the North American Regional Reanalysis (NARR), the Climate Forecast System Reanalysis (CFSR), the Modern-Era Retrospective analysis for Research and Applications Version 2 (MERRA-2), and the fifth generation of ECMWF Reanalysis (ERA5) for a 37-year period (1982-2018). Their temporal and spatial resolutions are listed in Table 2. We performed a point-to-point comparison between the blh calculated from the NAME rawinsondes and the blh obtained from the four reanalyses using a nearest neighbor approach.

Table 2. Reanalysis datasets.

Dataset	Spatial resolution	Temporal resolution	Vertical Levels	Reference
NARR	~ 32 km	3 hour	45	North American regional reanalysis
CFSR	~ 34 km	6 hour	64	The NCEP climate forecast system reanalysis
MERRA-2	~ 62 km	1 hour	72	The Modern-Era Retrospective Analysis for Research and Applications, Version 2 (MERRA-2)
ERA5	~ 27 km	1 hour	137	The ERA-Interim reanalysis: Configuration and

				performance of the data assimilation system

Finally, daily mean precipitation estimates from the Climate Hazards Group Infrared Precipitation with Station data (CHIRPS), which is a land-only climatic database with a spatial resolution of 0.05° (Funk et al., 2015), is used in this paper to identify the monsoon onset date. This data is also used to determine the spatial correlations between the blh of the GoC and monsoon precipitation. CHIRPS has been shown to have a very realistic annual precipitation cycle in the NAM region (Cavazos et al., 2019). Also, we performed a spatial verification of CHIRPS against the NAME Event Rain Gauge Network (NERN) daily data (Gochis et al., 2007). The CHIRPS precipitation data showed fair quantitative and spatial agreement with NERN (not shown here). We only noted a small northward displacement of the CHIRPS precipitation maxima.

2.3 The monsoon onset date

We identified the monsoon onset date for each season between 1982 and 2018. First, we performed an empirical orthogonal function (EOF) analysis on the daily mean precipitation values from CHIRPS. The EOF analysis (not shown here) was used to determine the areas of similar spatial precipitation variability from May through September. The first EOF mode suggested the blue polygon drawn in Fig. 1a. This polygon lies within the continental NAM core region as defined by Gutzler (2004), and is located along the western slopes and peaks of the SMO, which is the region of maximum climatological precipitation.

We calculated the average daily precipitation within that polygon for every year between May 1 and September 30. The monsoon onset for each year was defined as the date of the first day of the first sequence of five consecutive days with an average precipitation rate in the polygon equal to or greater than 2 mm/day.

2.4 The boundary layer height estimation from soundings

The methods addressed in Seidel et al. (2010) for the estimation of the mixing layer height from radiosonde data using potential temperature, relative and specific humidity, and refractivity profiles were tested to calculate the blh in the NAME dataset from the Ulloa cruises. As expected and is noted in Wang and Wang, 2014, the traditional methods resulted in inconsistencies and failed to produce a reliable estimation of the blh in over 80% of the NAME soundings, per visual verification. We therefore calculated the GoC NAME blh following an ad hoc three-step method based on temperature and relative humidity profiles, adapted from the recommendations and the comprehensive method for the mixing layer height estimation proposed by Wang and Wang 2014, but excluding the effects due to the presence of clouds.

Step 1. A 1-2-1 smoothing function is applied to all the temperature and humidity profiles to minimize the effect of extreme values, as recommended by Wang and Wang (2014).

Step 2. The altitudes of the three smallest vertical gradients of humidity and the three largest vertical gradients of temperature are recorded to identify the entrainment zone, which is the top of the boundary layer.

Step 3. The altitudes of the extreme-gradient layers determined above were compared. Wherever these altitudes were correspondent in pairs we identified them as a match. If only one match was found per sounding, then the height of the top of the matching temperature inversion layer was defined as the blh for that sounding. If more than one matching height was found for a single sounding, then the strength of the temperature inversions were compared and the top of the temperature inversion layer that was at least 1.5 times greater than the rest was selected as the blh. If all the temperature inversion layers were similar in strength, then the blh was selected to be that of the lowest inversion top.

We tested this procedure on 90 NAME soundings and it resulted in 81 blh's that were correctly identified, per visual verification. A total of 78 rawinsonde soundings (only those launched between 22° and 26° N in the NAME Ulloa cruises) were selected for the description of the vertical structure of the GoC boundary layer in the present study.

2.5 Richardson number calculations

To investigate turbulence in the boundary layer we calculated the bulk Richardson Number (BR; eq. 1), using 41 NAME rawinsonde soundings from the Ulloa cruises (only those that measured wind).

$$BR = \frac{\frac{g}{\langle T_v \rangle}\Delta\theta_v . \Delta z}{(\Delta U)^2 + (\Delta V)^2}, \tag{1}$$

In this equation g is acceleration due to gravity, $\langle T_v \rangle$ represents the average virtual temperature of the layer, $\Delta\theta_v$ is the virtual potential temperature difference across a layer of thickness Δz (vertical depth) and $(\Delta U)^2, (\Delta V)^2$ are the changes in the horizontal wind components across the same layer.

Since the BR number indicates only the presence of turbulence and not its intensity (Stull 2012), the results might be misleading when its values are averaged vertically over a layer. For example, the average of three contiguous BR values, let's say -0.1, -0.01 and 3.5, is 1.13 which indicates an absence of turbulence (i.e. laminar flow). But actually, the vertical layer over which those three numbers were averaged is more turbulent than laminar. To overcome this issue, we introduced an adjusted bulk Richardson Number (ABR) that allows a clearer distinction between turbulent and laminar layers when using average BR values, as follows:

ABR = -1.0 if BR ≤ 0.25

ABR = 0.0 if 0.25 < BR < 1.00

ABR = 1.0 if BR ≥ 1.00

Vertical averages using ABR can be interpreted as follows:

The layer is dynamically unstable (turbulent) if ABR ≤ -0.5,

The layer is dynamically stable (not turbulent) if ABR > 0.5, and

The layer has stably stratified turbulence if -0.5 < ABR ≤ 0.5.

3 Results and Discussion

First, we analyze the temperature (T), relative humidity (Rh), and zonal wind component (u) mean vertical structure within the boundary layer using the NAME rawinsonde and PIBAL data. The differences in the diurnal cycle before and after the monsoon onset that are implied by our analysis are summarized in vertical cross section sketches of atmospheric circulation taken through the NAM core region. A detailed analysis of the gulf blh is presented, which includes a comparison between four different reanalysis datasets. Using the observational ABR estimations, we investigate turbulence generation to identify the physical processes responsible for the mixing of the GoC boundary layer in the context of the NAM onset. Finally, we present a spatial significance analysis of the relation between the mean blh of the GoC after the monsoon onset and the subsequent precipitation over the surrounding landmass.

3.1 Vertical structure of temperature, relative humidity and zonal winds in the Gulf of California boundary layer.

The reader should first realize that the following description of the GoC boundary layer structure is strictly representative only of the southern region of the gulf (between 22 and 26 °N approximately), as the data was obtained from rawinsondes in that area. It’s possible that the boundary layer behaves differently in the northern region of the gulf.

Fig. 2 presents the average day and nighttime temperature and humidity profiles for the June (pre-onset) and August (post-onset) 2004 NAME marine rawinsonde dataset. For the daytime profiles, the soundings launched between 0600 and 1800 LT were averaged; for the nighttime profiles, the rest of the launches were considered. The average surface layer (ASL) was visually identified; the solid horizontal line in the figure represents the computed mean mixed layer.

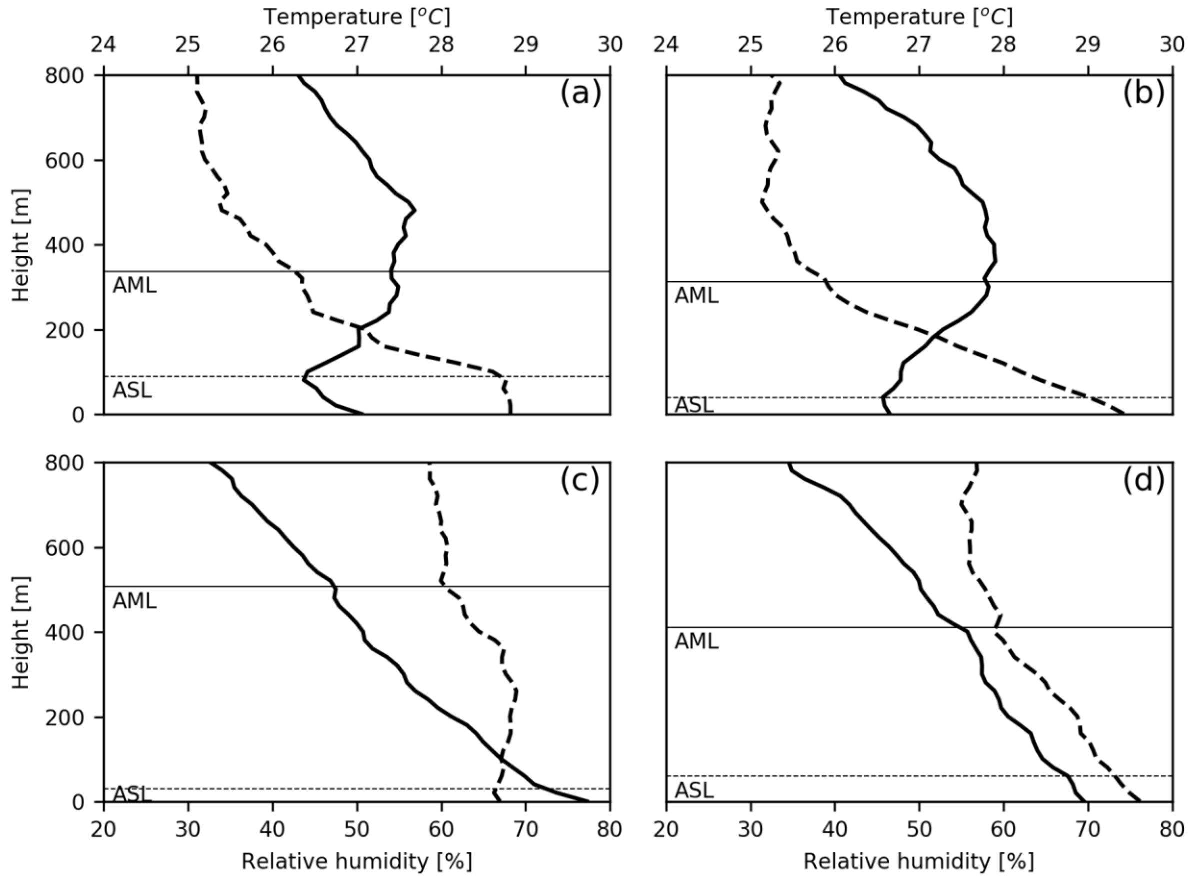

Figure 2. Mean vertical profiles of temperature (solid curves) and relative humidity (dashed curves) from the 2004 NAME rawinsondes dataset. **(a)** June daytime soundings; **(b)** June nighttime soundings; **(c)** August daytime soundings; and **(d)** August nighttime soundings. AML is the average mixed layer height (horizontal solid line) and ASL is the average surface layer height (horizontal dotted line).

The differences between the June and August temperature profiles are noteworthy. The day- and nighttime boundary layers before monsoon onset (June profiles) are stable, with humidity decreasing rapidly with height. The June blh is characterized by minimal daily variations due to compensation from thermodynamical and mechanically driven processes. Downward air movement over the gulf is expected to compete against the positive buoyant force generated by surface heating during daytime (Badan-Dangon et al., 1991). Since the boundary layer is stable and the thermal inversion over the gulf is present, all the energy produced by heating and evaporation is retained in the surface layer, which is thick and very well mixed. After sunset, the inversion weakens and air convergence over the gulf overcomes stability sufficiently to inject part of the energy stored in the surface layer into the boundary layer.

This picture is very different in the August profiles. After the onset, the day and nighttime mean vertical profiles imply instability due to an increase of the surface temperature of up to 3 °C relative to the June profiles. The increased positive buoyancy force favors mixing, effectively injecting most of the surface water vapor aloft during the daytime. Consequently, the surface layer is thin while the boundary layer thickens against the subsiding air. During the nighttime, the instability-producing buoyancy force decreases due to radiative cooling while low-level convergence occurs over the gulf (see nighttime plots of Fig. 3). However, there is no energy left to inject into the boundary layer, and the blh decreases.

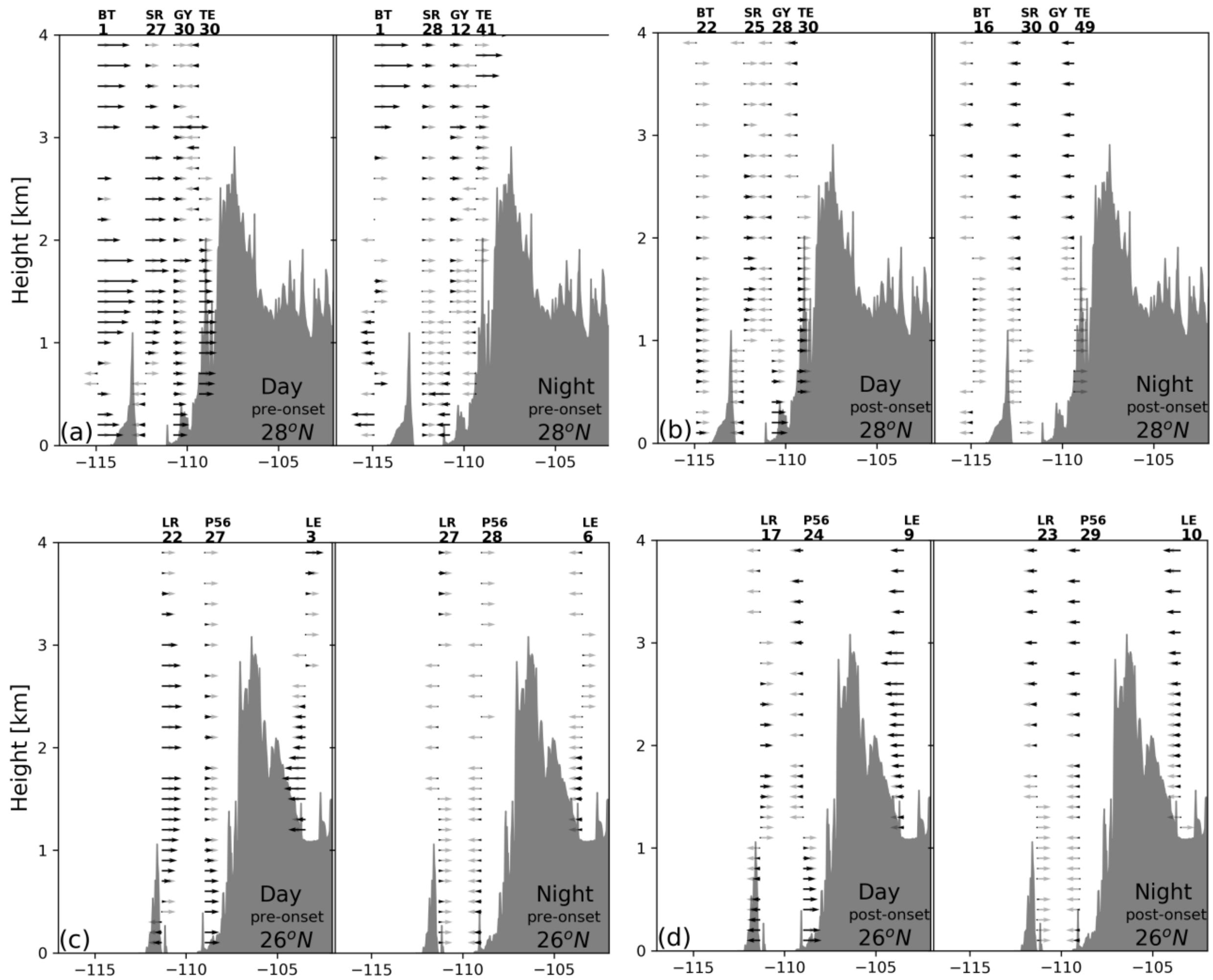

Figure 3. Day (left) and nighttime (right) longitude vs. height cross-sections of the average cross-gulf wind component observed at NAME PIBAL stations for latitudes: **(a, b)** ~28 ^{o}N and **(c, d)** ~26 ^{o}N. Plots **(a, c)** correspond to June 2004 (pre-onset) averages while **(b, d)** are August 2004 (post-onset) averages. Black arrows indicate the average cross-gulf wind component (u rotated according to the gulf axis: 325 °), while the gray arrows are normalized vectors included to aid the visualization of flow direction. Numbers at the top indicate the total of data profiles averaged for each station; black letters are abbreviations for each station name (see Fig. 1a). Corresponding Shuttle Radar Topographic Mission 3 arc second (SRTM-3) topography profiles are shaded.

It appears that thermodynamics plays an essential role in the observed behavior of the GoC boundary layer. Temperature changes and evaporation determine the type of stability and, by extension, whether the vertical motion is enhanced or counteracted. On the other hand, horizontal winds can also affect the temperature and water vapor variations. For example, the surface relative humidity is always higher at nighttime (before and after the monsoon onset) than during daytime because of cold advection from the land breeze that destabilizes the surface layer (Arya 2001), thus intensifying the water vapor flux from the gulf.

To study the vertical distribution of the zonal winds, two vertical cross sections were taken at 26 and 28 °N (yellow dotted lines in Fig. 1a). For each of these cross sections, vertical wind (u) profiles, rotated to a frame of reference that coincides with the gulf axis (325 °), from the NAME PIBAL stations closest to each latitude were averaged for the pre-monsoon onset (June) and post-onset (August) conditions (see Fig. 3; the SRTM-3 topographic data is also included). In this figure, a number indicating how many soundings were averaged at each PIBAL station is displayed at the top of every profile. The June averages for the Bahía Tortugas (BT) and Lerdo (LE) stations must be interpreted with caution due to the low number of available profiles.

Two distinct diurnally dependent, thermally driven circulations coexist over the GoC: a complex land/sea breeze and mountain winds, due to zonal interactions between the Pacific Ocean, the BC peninsula, the gulf and the SMO. During the day, the land surface is warmer than the water surface. Consequently, there is an onshore flow on both coasts of the BC peninsula and on the continental Mexico coastline as well. These sea breezes interact with the topography of BC and the SMO, producing convergence over the peninsula and divergence over the GoC. However, as the Pacific Ocean to the west of BC is cooler than the gulf, and also because the SMO has a more prominent slope, the circulation is stronger over the western coast of the peninsula and over the mainland coast. The onshore flow from the GoC to BC can clearly be seen in the daytime plots of Figs. 3a, d. This flow was not observed in the cross-gulf transects presented in Johnson et al. (2010), probably due to their data resolution. Furthermore, a weak return flow aloft can be seen over the western coast of the gulf, with the wind direction changing from easterly to westerly at a height of around 550 m before the onset and 1100 m after the onset (see profiles over the western GoC in the daytime panels of Figs. 3a,d). This circulation is expected to close with subsidence over the central gulf.

During nighttime, the land surface is cooler than the water surface and the circulation reverses as downslope-offshore flows set up. In general, the low-level circulation tends to be weaker at night due to the weaker thermal gradients. The mountains cool by long-wave radiation and the chilled air descends downslope and converges over the gulf. This convergence is found from the surface to nearly 1200 m height over the GoC and up to 1800 m above sea level over mainland (approximately at 110° W longitude) due to the complexity of SMO mountain system; see Fig. 3a at night. The near-surface land breeze off of the mainland, as shown by the GY and P56 PIBAL stations in the nighttime plot of Fig. 3d, was not observed in Zuidema et al. (2007) probably because the soundings they used were launched near the center of the GoC's mouth, approximately 80 km from the mainland and peninsula coasts. Additionally, it must be noted that there is a large topographic gap in the BC peninsula near 24 °N (see Fig. 1b). This orographic feature causes that, at low levels, the temperature difference between the Pacific Ocean and the GoC dominates the diurnal wind field. In fact, Turrent and Zaitsev (2014) identified nocturnal and early morning breeze flows from the Pacific Ocean to the GoC related to the temperature difference between these two bodies of water connected by a narrow cross-section of the peninsula with low topography.

The wind circulation over the mainland Mexico coast is generally weaker after the monsoon onset, possibly due to a decrease in the land surface heating caused by the increase of moisture (Ciesielski and Johnson 2008). At higher levels, a shift in the zonal wind direction that is due to the northward displacement of the monsoon mid-level anticyclone can be noted before and after the onset, switching from westerly to easterly.

In Fig. 4, two circulation sketches are drawn for before (a) and after (b) the monsoon onset, highlighting the features mentioned above. For these sketches we used only the PIBAL data shown in Fig. 3. The continuous black lines represent real PIBAL data while discontinuous lines depict inferred flow. The gray shaded areas represent the real SRTM-3 topography data at 26 °N. The positive and negative signs at the bottom of the plots symbolize the presumed surface heat fluxes of the surrounding lands and the ocean, relative to the pre-onset daytime warming of the GoC.

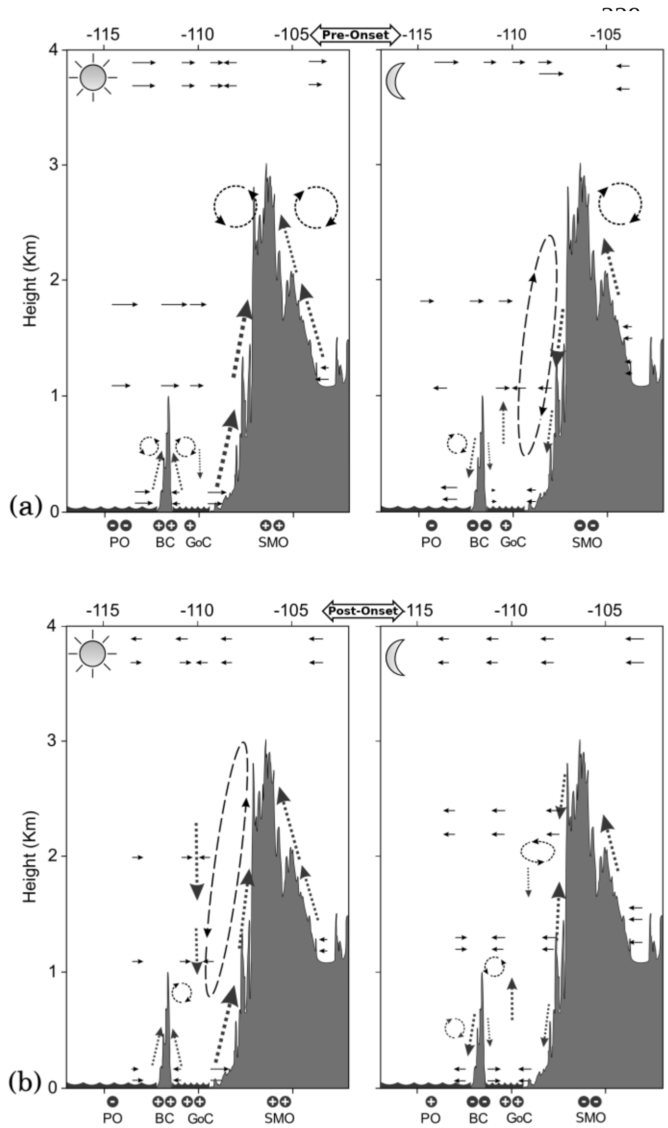

Figure 4. Schematic vertical cross sections (longitude vs. height) of circulation deduced from the mean cross-gulf wind observed at NAME PIBAL stations located near 26 °N. **(a)** Pre-monsoon onset day (left) and nighttime (right) conditions; **(b)** post-monsoon onset day (left) and nighttime (right) conditions. Discontinuous lines depict the inferred flow.

The circulations proposed in Fig. 4 highlight the changes in the large scale, mean zonal wind direction in the middle troposphere before and after the onset, and its impact on the circulation cells depicted in the lower levels. Before the monsoon starts, the air that is moving from the gulf towards the peninsula with the daytime sea breeze rises and has a return flow at a height of ~500 m, where it encounters the free-atmosphere westerly winds. The subsidence that occurs over the gulf is likely due to this return flow. Before the onset, the sea breeze cell over the gulf is asymmetric and is only present over the western (peninsular) side of the GoC (left panel of Fig. 4a). But once the monsoon starts, a second larger daytime circulation cell forms over the continental side and the subsidence layer above the gulf thickens up to 3000 m (left panel of Fig. 4b). This larger cell presumably merges with the more persistent mountain breeze cell near the SMO peaks.

The largest circulation cell that forms during the day after the onset weakens during nighttime. In the right panel of Fig. 4b, the small circulation cell that persists on the eastern side of the gulf at a height of ~2 km is possibly a residual flow from the daytime cell which contributes to nighttime precipitation or cloud formation. On the eastern side of the SMO Mountains, the return branch of the circulation cells at the highest elevations only appears before the monsoon onset and there is no clear sign of persistent mountain breeze systems as the air rises mostly by mechanic forcing, as reported by Johnson et al. (2010).

Before the onset, the largest circulation cell located over the eastern gulf also tilts towards the SMO mountain slopes, but seems to be present only during nighttime (Fig. 4a, right panel) and flows in the opposite sense, due to the effect of the nocturnal land breeze and the convergence generated over the central gulf.

In general, we note that the complex circulation over the GoC exhibits several features that can cause vertical and horizontal wind shear. The asymmetry of the terrain elevations on both sides of the gulf and the fact that upslope and downslope air parcels don't ascend or descend entirely but rather spread horizontally at their level of neutral buoyancy are critical to these features.

3.2 Spatial and temporal evolution of the Gulf of California boundary layer height

The black solid curve in Fig. 5 plots the mean blh of the GoC calculated from the NAME rawinsonde data with the method addressed in section 2d. The mean blh increases approximately 150 m after the monsoon onset. Before the onset (top panel), there is not much difference in the thickness of the boundary layer between day and night. The latter happens because the boundary layer experiences an unusual development during night hours. Typically, the boundary layer thickens with solar heating during the daytime and it becomes shallow at night due to the stability of the surface layer (Liu and Liang 2010). Note that the average nighttime (2200 and 0400 LT) and daytime (1000 and 1600 LT) blh is between 300-350 m, which is only slightly higher than the heights reported by Badan-Dangon et al. (1991).

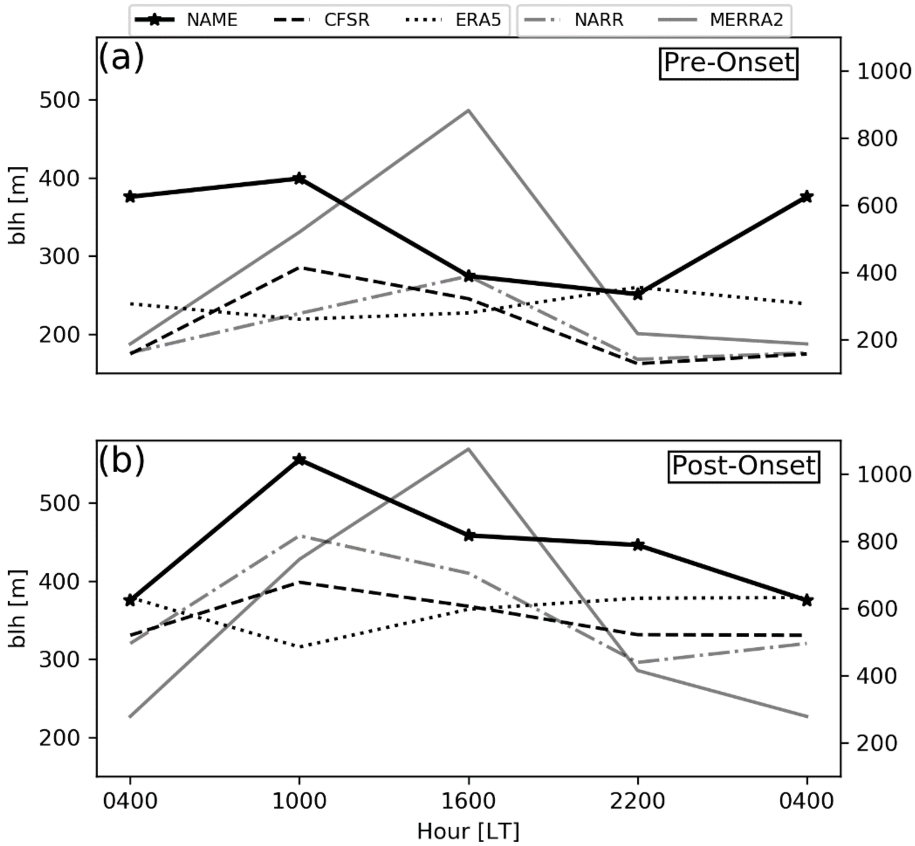

Figure 5. Diurnal cycle of boundary layer heights (blh) averaged **(a)** before and **(b)** after the 2004 monsoon onset; estimates from the NAME rawinsonde dataset (black solid) and from the CFSR (black dashed), NARR (gray dash-dot), ERA5 (black dotted), and MERRA-2 (gray solid) reanalyses. NARR and MERRA-2 data are plotted using the right y-axis.

The observed blh (black solid in Fig. 5) reaches its daily maximum at 1000 LT, both before and after the NAM onset. The minimum height occurs at 2200 LT before the onset and shifts to 0400 LT after the monsoon begins. This diurnal cycle is being modulated by two factors simultaneously: the breeze regime described in Fig. 4 and the thermal inversion found by Erfani and Mitchell (2014). The blh extreme values are directly related to the breeze regime, while the beginning of the nocturnal growth of the boundary layer depends on the presence and intensity of the inversion. During nighttime, surface winds converge over the gulf and the boundary layer grows until subsidence develops aloft beginning at around 1000 LT. As the subsidence intensifies, the blh decreases, reaching its minimum value between 2200 and 0400 LT.

Before the onset, we hypothesize that the thermal inversion over the GoC persists throughout the diurnal cycle because the gulf's surface is not warm enough to break it. The inversion likely intensifies during the day and weakens -without breaking- at night due to the effect of the breezes. The inversion layer acts as a lid keeping the humid air trapped within the boundary layer. When subsidence over the gulf begins to fade around 2200 LT, part of the convective energy releases and the boundary layer starts growing. However, once the monsoon begins the thermal inversion has faded away and the nocturnal growth starts at later hours (0400 LT), owing to the surface convergence over the gulf.

Four reanalysis datasets (CFSR, NARR, ERA5 and MERRA-2) were used to compare the blh estimates of the GoC; see Fig. 5. This comparison was made for the same time period and area covered in the NAME dataset. All four reanalyses capture the increase in the mean blh after the monsoon onset. However, CFSR (black dashed line) has the smallest bias and also captures the nocturnal growth of the boundary layer before the onset. Meanwhile, ERA5 (black dotted line) underestimates the blh and has a diurnal cycle that behaves inversely to the one seen by the observations. MERRA-2 (gray solid line) has the largest bias and doesn’t capture well the diurnal evolution of the blh. The NARR (gray dash-dot line) estimates are in good agreement with the observed evolution of the blh after the onset, but with a notable overestimation of the values. Overall, CFSR gives the best estimates of the blh both before and after the onset.

The June 2004 monthly averaged near-surface (1000 mb) horizontal divergence fields for the four reanalyses are shown in Fig. 6. Results are presented for the same hours analyzed in Fig. 5. These wind divergence fields illustrate the evolution of the local breeze systems over the GoC region and the comparison between the reanalyses illustrates why the CFSR blh estimation is the most accurate. Blue colors in Fig. 6 are associated with divergence (positive values) in the near-surface wind field while red colors represent convergence (negative values).

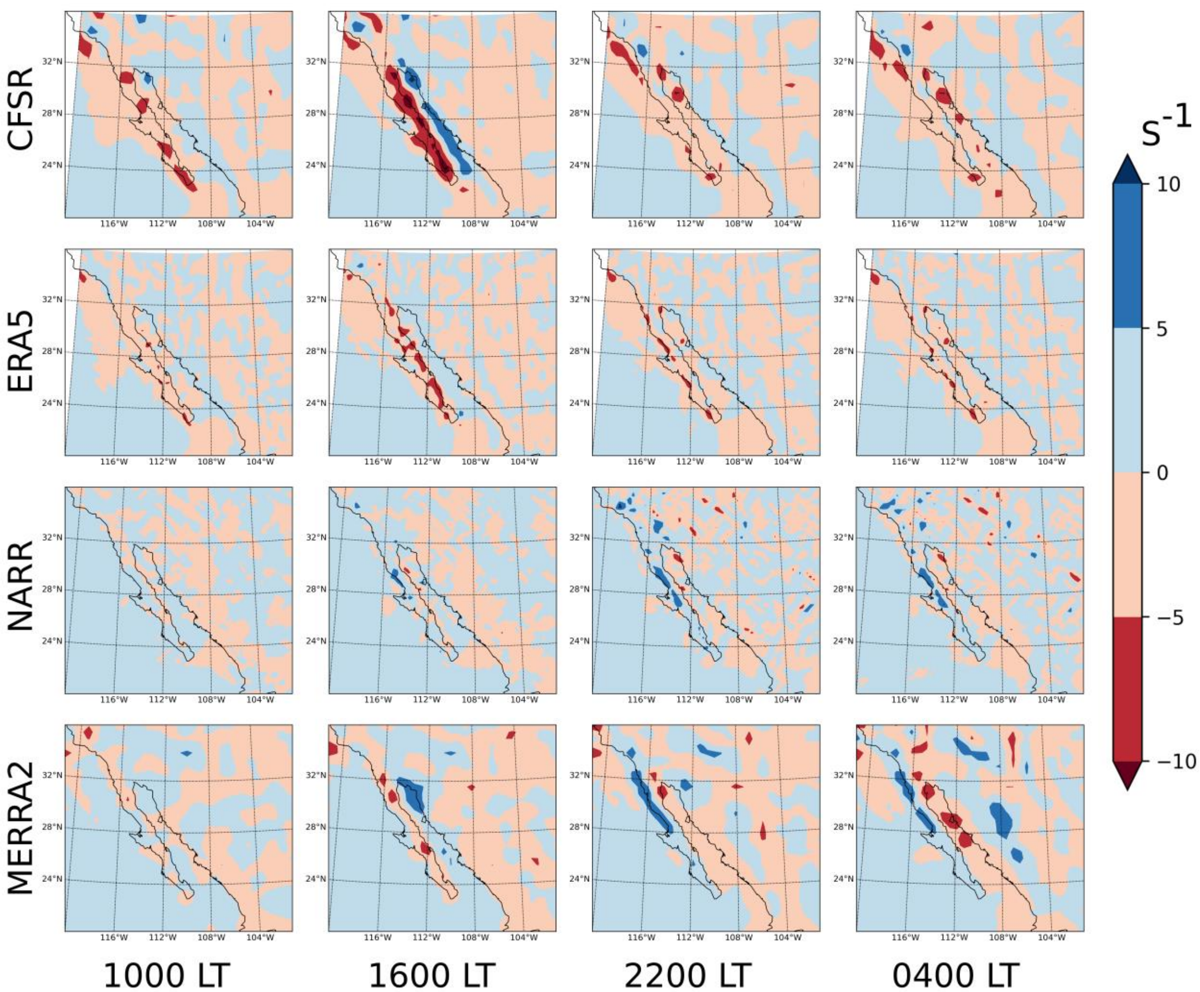

Figure 6. June 2004 near-surface (1000 mb) monthly mean horizontal wind field divergence computed (from top to bottom) from CFSR, ERA5, NARR and MERRA-2 at (from left to right) 1800, 0000, 0600 and 1200 UTC.

The sign of the wind field divergence over the gulf changes from negative to positive values between 0400 and 1000 LT. The pattern is seen in all the reanalyses, but the signal is stronger in the CFSR (top panels in Fig. 6). It's reasonable to assume that this change towards divergence is associated with the start of the landward propagation of the sea breeze over both coasts. It also signals the initiation of the related subsidence over the gulf during daytime hours. This change would then also explain why the boundary layer reaches its maximum height at 1000 LT.

As seen in Fig. 5, the boundary layer starts to grow at 2200 LT because convergence sets in over the gulf, and its development ends at 1000 LT when the near-surface wind field becomes divergent. The blh decreases to its minimum at 1600 LT when the divergence over the GoC is strongest. Our analysis did not find significant differences in the diurnal cycle before (Fig. 6) and after (figure not shown) the onset.

When comparing the reanalyses we noted that CFSR and ERA5 have similar behaviors, with CFSR having more intense gradients in the GoC region. NARR and MERRA-2 represent the effects of the BC peninsula differently, as can be seen by the spatial displacements of the local extremes. Overall, it appears that CFSR is more physically consistent as it better explains the evolution of the GoC boundary layer. Still, the horizontal spatial resolution of the CFSR limits is use in the study of the regional breeze regimes. Further work with a higher spatial resolution is needed; e.g., a dynamical downscaling of the CFSR fields thru use of a regional model at a resolution higher than 4 km. Nevertheless, given that by comparison between observations and several reanalyses the CFSR blh proved to be the most reliable, we propose it is also suitable for the investigation of the interannual fluctuations of the GoC boundary layer.

Fig. 7 presents the interannual variability of the average daily precipitation and the monsoon onset date, according to the procedure defined in section 2c using the CHIRPS dataset. Once the onset date was determined for each year in the study period, average daily precipitation was calculated for the first 30 days after the onset over the blue polygon shown in Fig. 1a.

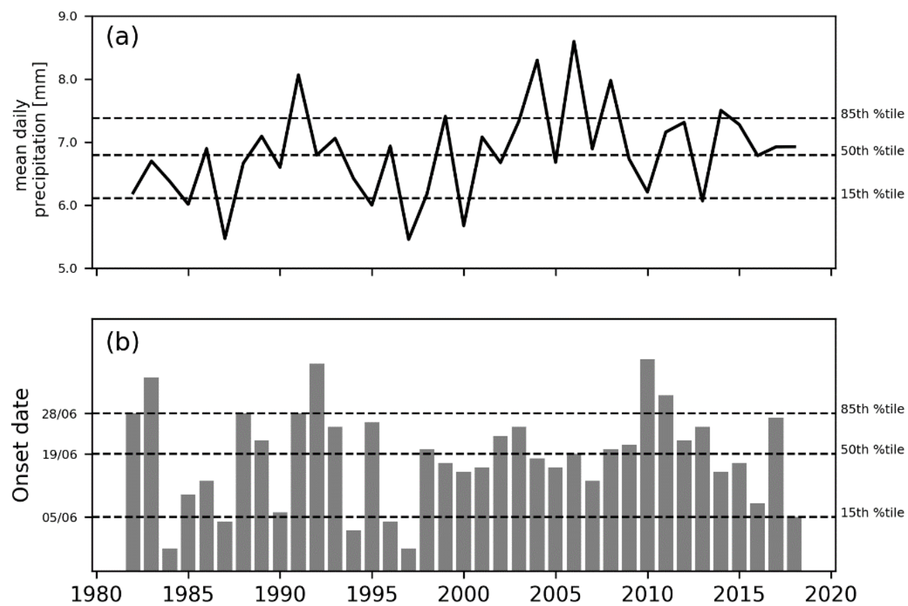

Figure 7. Interannual variability of the **(a)** mean daily precipitation [mm] calculated using the white polygon in Fig. 1a during the first 30 days after the NAM onset, and **(b)** the NAM onset date for the core region, from 1982 to 2018. The dashed lines represent the 15th, 50th and 85th percentiles of the time series.

The average onset date for the period 1982-2018 in this study is June 19. Xu et al. (2004) used a threshold of average precipitation above 2 mm/day for three consecutive days in the Southern SMO (22°–24°N, 104°–106°W) and Central Mexico (25°–27°N, 106°–108°W) regions. Their average onset date was June 20 for the period 1980-2001. Also, Higgins et al. (1999) used a criterion of 1.0 mm for five consecutive days and determined that the average onset date between 1963 and 1988 for northwestern Mexico was June 17.

The years with mean daily precipitation below the 15th percentile (6 out of 37 years) were classified as “dry” years in Fig. 7a. Above the 85th percentile, six other seasons were classified as “wet” years, and the rest (25 years) were considered “average” seasons. Similarly, the years with an onset date below the 15th percentile (6 out of 37 years) were classified as having an “early” onset in Fig. 7b. The seven years at or above the 85th percentile were classified as having a “late” onset and the 24 years in between both lines were considered as having “average” onset dates.

The correlation between these two variables: the onset date and the average daily precipitation over different time windows for the period 1982-2018 is shown in Fig. 8. The maximum time window considered is 90 days, which was three months after the onset. In this figure positive correlation values indicate that during a given time window, early onsets are related to a drier outcome and late onsets to wetter conditions. Higgins et al. (1999) and Douglas and Englehart (1996) showed that monsoons with early onsets are expected to have more precipitation than monsoons with late onsets because monsoons that start earlier should last longer. In Fig. 8 this behavior is found for time windows of more than 80 days, when correlations become negative. However, Fig. 8 also shows that for the first 80 days after the monsoon starts, early onsets are associated with less precipitation while late onsets accumulate more precipitation during the same time period. Positive correlations above 0.5 were found for the period between 20 and 40 days after the onset; the highest value is 0.58 with a p-value < 0.01, which implies a moderate direct relationship with high statistical significance (> 99 %). For these time windows a late onset implies a wetter start, while early onsets are associated with drier conditions. We hypothesize that this occurs because the longer a monsoon onset is delayed the greater amount of convective energy is stored in the boundary layer, being kept there by the thermal inversion over the GoC. Once the surface temperature of the gulf is enough to break the inversion, the low-level gulf accumulated moisture is released and becomes available for monsoon precipitation.

This statement is based on the premise that both the seasonal warming of the GoC’s surface water and the thermal inversion that caps its boundary layer vary in intensity and timing from one year to the next. A stronger inversion layer would require higher sea surface temperatures (SSTs) to be eroded, and the longer it takes to be broken, the more moisture is accumulated in an increasingly higher boundary layer. A correlation analysis between the gulf daily SST provided by the National Oceanic and Atmospheric Administration (Reynolds et al., 2007) and the daily-averaged blh from CFSR, both spatially averaged over the black polygon in Fig. 1a, was performed for the time period 1982 to 2018. The highest correlation between those variables was found to be 0.76 (significant at 95 %) when a time-averaging window of 40 days centered on the monsoon onset date was used to calculate the yearly value for each variable. Shorter (6 days) and longer (60 days) time-averaging windows produced correlations ranging between 0.68 and 0.74 (significant at 95 %). The heat budget analysis by Castro et al (1994) established that the GoC warms during the summer as a result of the heat advected into it from the Pacific Ocean (and not through its net surface heat flux). Our results imply that the ocean processes responsible for the interannual variability of that heat advection, which likely involve the dynamics of semiannual internal waves that originate at the equator (Gómez-Valdivia et al. 2015), are also relevant for the interannual modulation of the NAM.

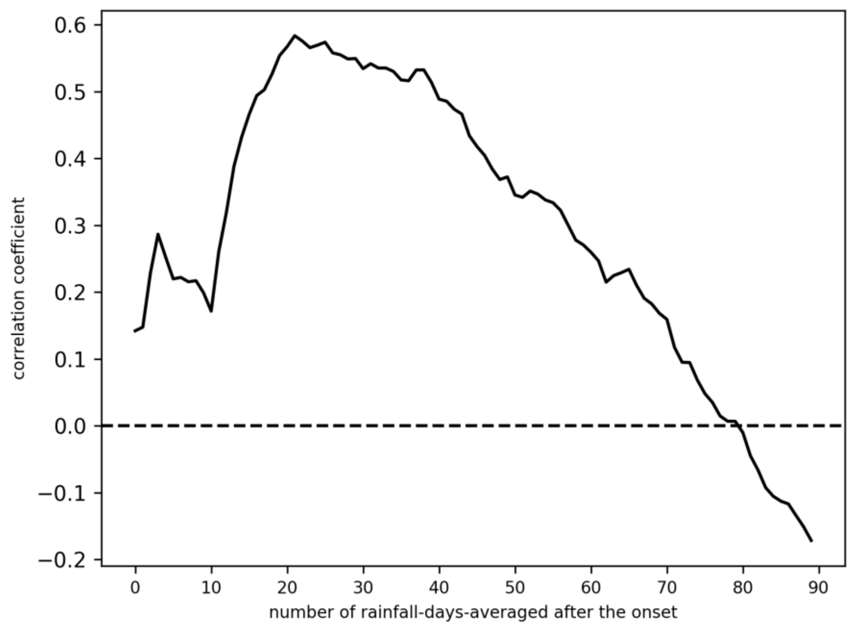

Figure 8. Correlation coefficients calculated between the daily mean precipitation in the core region time-averaged over different time windows and the monsoon onset date, from 1982 to 2018.

3.3 Mixing of the Gulf of California boundary layer and the NAM onset

As mentioned above, we used 78 soundings of the NAME experiment to examine the GoC boundary layer. However, only 41 of these soundings contained wind measurements. This lack of information certainly makes calculating the Richardson Number difficult (Erfani and Mitchell, 2014). Even so, this analysis can be helpful to understand how mixing occurs in the gulf boundary layer. Flows with Richardson Numbers (BR) higher than 1.0 are said to be statically stable, while those with BR < 0.25 are statically and dynamically unstable. However, flows in the range of 0.25 < BR < 1 can still be turbulent depending on their history (Stull 2012). We used (1) to estimate the BR values shown in Fig. 9 (continuous curves), averaged within the boundary layer. When BR drops below the critical value BRC = 0.25 the boundary layer increases its height because the flow becomes turbulent. This feature of Fig. 9 indicates that our estimation of BR is indeed meaningful in the context of the blh diurnal cycle of the GoC, despite the reduced number of available soundings with wind data.

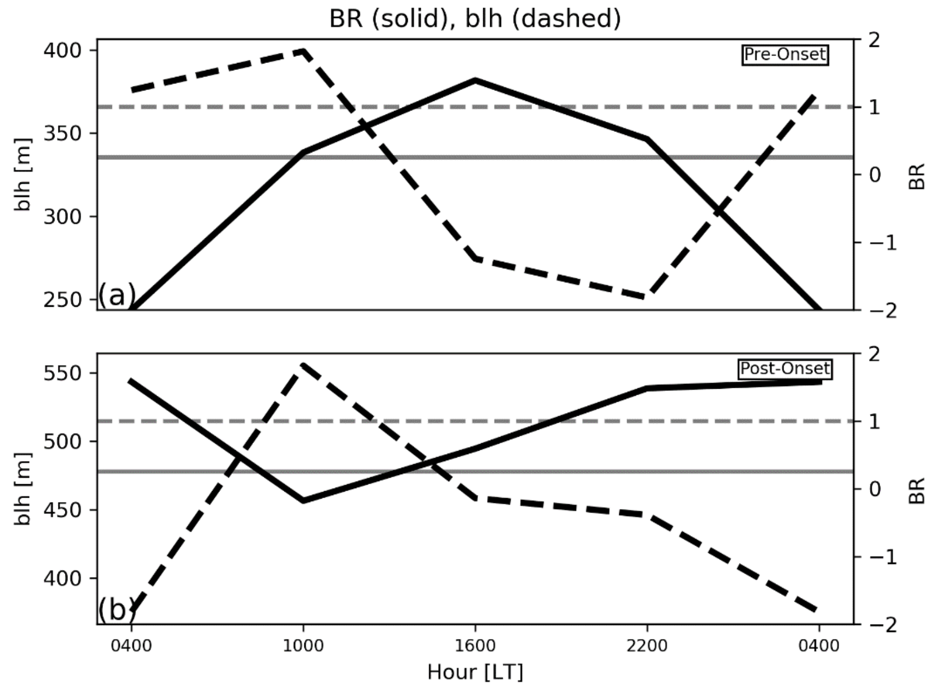

Figure 9. Time variation of the Bulk Richardson Number (BR , continuous curve) and the boundary layer height (blh, discontinuous curve) from 2004 NAME rawinsondes: **(a)** before the monsoon onset and, **(b)** after the monsoon onset. The critical value BRC =0.25 (gray solid line) and termination value BRT =1.0 (gray dashed line) are also shown.

By taking a closer look at the variation with height of the adjusted Richardson Number (ABR, Fig. 10a), it's possible to identify the layers that are dynamically unstable on average, and hence, where and when turbulence occurs. The dotted line represents the average height of the day and nighttime boundary layer before and after the onset. Turbulent layers are shaded in light-gray while the stable layers are indicated in gray.

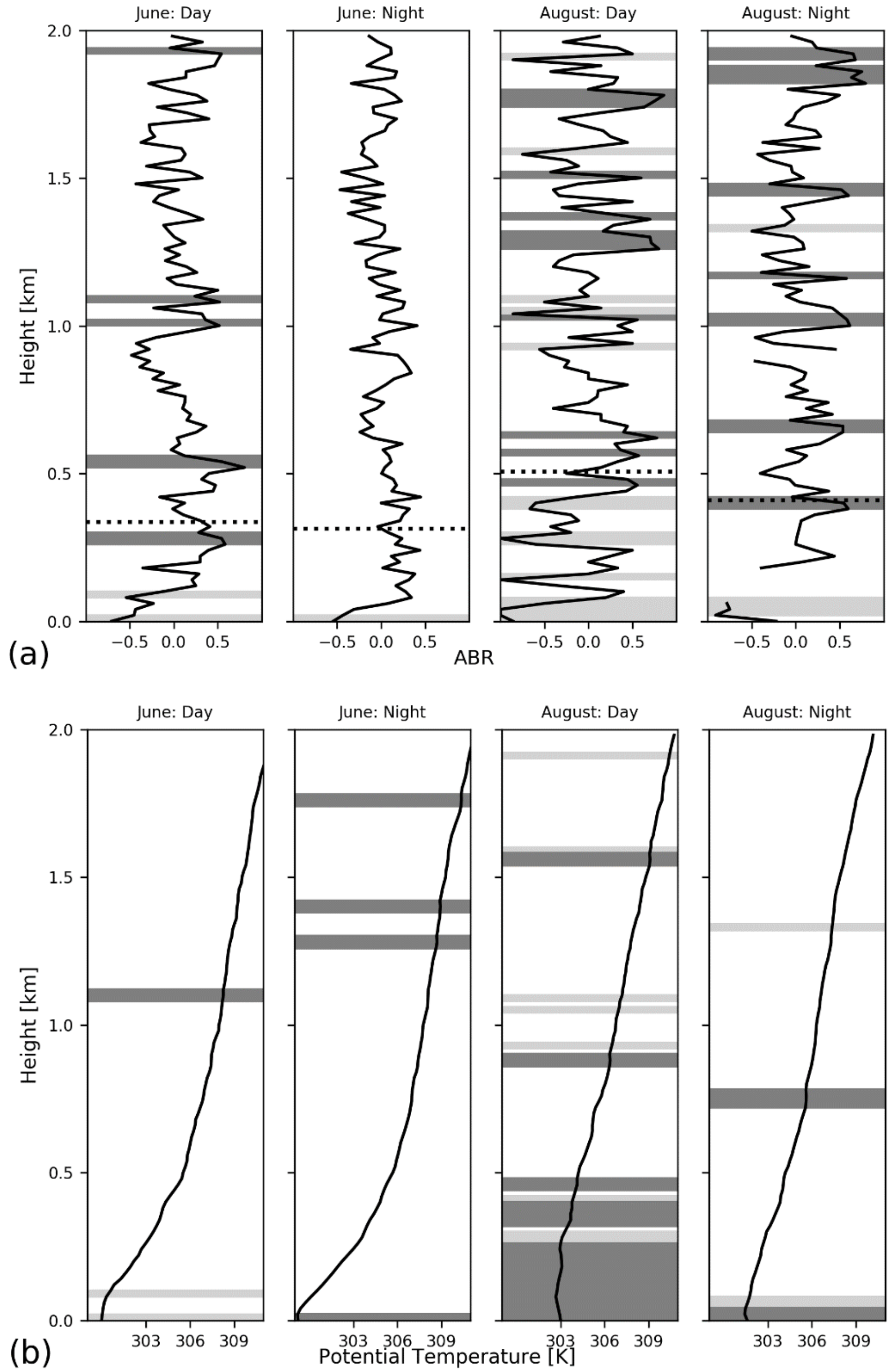

Figure 10. Turbulence layers identified for mean 2004 NAME rawinsondes. **(a)** Vertical profiles of the mean adjusted Bulk Richardson Number (ABR, black lines). The shaded layers identify dynamic turbulent flows (light-gray) and dynamic laminar flows (gray); white layers represent stably stratified turbulence. The dotted lines indicate the corresponding mean boundary layer height. **(b)** Potential temperature profiles (θ, black lines). The shaded areas represent the dynamic turbulent layers (light-gray) and the non-local statically unstable layers (gray). From

left to right, the plots correspond to: June daytime, June nighttime, August daytime and August nighttime.

We found that turbulent layers are relatively thin and are scattered throughout the air column. Also, these dynamically unstable layers are more commonly present after the onset and during the daytime. During June daytime (pre-onset conditions), the unstable layers were found below 100 m and were further restricted to below 40 m during the nighttime because of the stability of the boundary layer. Note that in statically stable boundary layers, the buoyancy term consumes turbulent kinetic energy (TKE) by converting it to potential energy as cold air ascends and warm air descends (Stull 2012). During August daytime (post-onset conditions) the turbulent layer adjacent to the surface thickens, while several other thinner layers appear at different heights because of the increased heating. During August nights the number of turbulent layers decreases (in relation to daytime) and the lowest turbulent layer was observed to be detached from the surface, possibly due to radiative cooling. It is interesting to note that the mean blh is usually very close to the lowest laminar layer, which gives confidence to the accuracy of the proposed method for the calculation of the blh, as well as for the correct averaging of the bulk Richardson Number (ABR; see sections 2d, e).

Additionally, we examined the non-local static stability along with the BR Number (Fig. 10b) to identify the turbulent regions of the flow thoroughly. The method to determine the non-local static stability requires plotting the potential temperature (θ) profile and displacing parcels upward (downward) from the relative maximum (minimum) θ values (Wallace and Hobbs 2006). In Fig. 10b, the layers shaded in light-gray are the same turbulent layers shown in Fig. 10a, while the gray shades indicate the non-local static instabilities. The turbulent layers identified by our analysis are all the regions statically or dynamically unstable in Fig. 10b. When comparing the statically unstable layers (gray shades), the most notable difference was found between the June (Fig. 10b, first column), and August (Fig. 10b, third column) daytimes; the lowest 500 m of the boundary layer became statically unstable during the latter. Erfani and Mitchell (2014) emphasized that the seasonal warming of the gulf's surface produces a superadiabatic surface layer that intensifies the vertical mixing and removes, or at least weakens, the inversion. However, this is not the only mechanism mixing the boundary layer. As noted earlier, the production of dynamic turbulence also increases after the onset.

The origin of the dynamic turbulence can be determined by comparing the buoyancy and shear terms in the BR Number equation (1) using instantaneous sounding data. In Fig. 11 we investigate the turbulence within the gulf boundary layer by plotting the buoyancy (abscissas) and shear (ordinates) terms. The approximate regimes of free and forced convection are shown in the figure for June (top plots) and August (bottom plots) 2004 NAME rawinsondes (after Stull 2012). The hatched area (forced convection) lies in the range -0.25 <= BR <= 0.25, while the light-gray area for BR >= 1.0 indicates no turbulence and the gray shading (BR <= -4.0) represents free convection. The stably stratified turbulence ranging between 0.25 < BR < 1.0 and turbulence driven by shear and buoyancy (ranging between -4.0 < BR < -0.25) are also indicated in the figure. The percentage labels shown indicate the number of observations found in the database within each approximate regime relative to the total number of instantaneous sounding measurements in each plot.

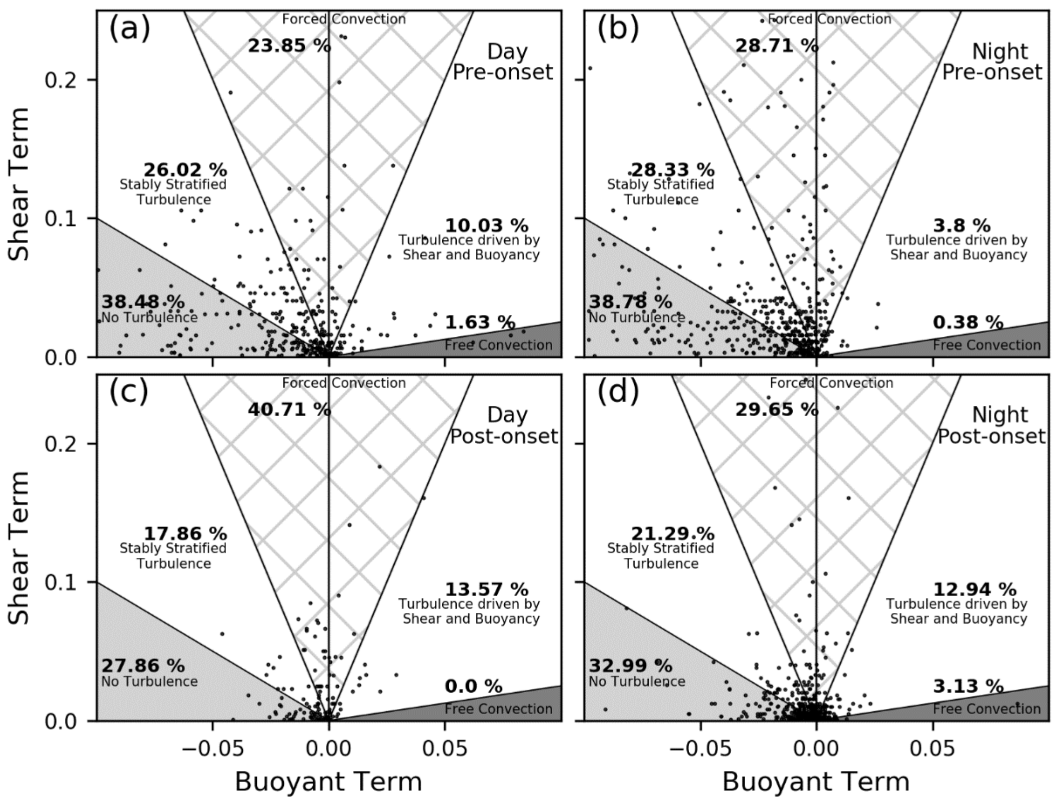

Figure 11. Approximate regimes of free and forced convection (adapted from Stull, 2012) for the 2004 NAME rawinsonde instantaneous observations: **(a)** June days, **(b)** June nights **(c)** August days and **(d)** August nights. The range -0.25 <= BR <= 0.25 is hatched, the light-gray shading accounts for BR >= 1.0 and the gray shading is for BR <= -4.0. The stably stratified regime lie between 0.25 < BR < 1.0, while the turbulence driven by wind shear and buoyancy corresponds to the range -4.0 < BR < -0.25. Percent of observations found for each regime are highlighted in bold.

Figure 11 highlights that the primary mechanism for the daytime mixing of the GoC boundary layer after the NAM onset is the turbulence produced by wind shear, as illustrated by the considerable increase found in the forced convection regime. During the nighttime, buoyancy also contribute to the mixing of the layer. Two requirements must be met to produce turbulence: the presence of instability and a triggering mechanism (Stull 2012). Before the NAM onset we have neither. On one hand the mean boundary layer is stable, which implies that all the mechanical production of turbulence is being consumed by buoyancy. And on the other hand, the gulf's surface temperatures are not high enough to provide the triggering mechanism necessary to erode the inversion and mix the boundary layer with air aloft. But once both conditions are met the monsoon progresses through its onset phase: the gulf's warming induces a superadiabatic surface layer (triggering mechanism) while wind shear continuously provides dynamic instabilities to maintain the turbulence and allow efficient mixing of the GoC boundary layer. It is important to note, however, that the analysis presented here must be regarded as strictly incomplete, as the approximations for only two terms of the TKE equation have been considered.

The other terms (advection, dissipation, etc.) must also be considered in future work. Especially the former, since advection of air due to the unique breeze regime over the gulf likely causes significant changes in the TKE budget.

3.4 Does the GoC boundary layer influence monsoon precipitation?

So far we have studied the GoC boundary layer as an essential element of the monsoon onset. It is reasonable to think that NAM precipitation after the onset is also related to the gulf boundary layer. To test that idea we analyzed the correlations between the CFSR blh and the CHIRPS precipitation during the first 15 (Fig. 12a) and 30 days (Fig. 12b) of each monsoon season, from 1982 to 2018. The area-averaged daily blh was calculated for the black polygon shown in Fig. 1a.

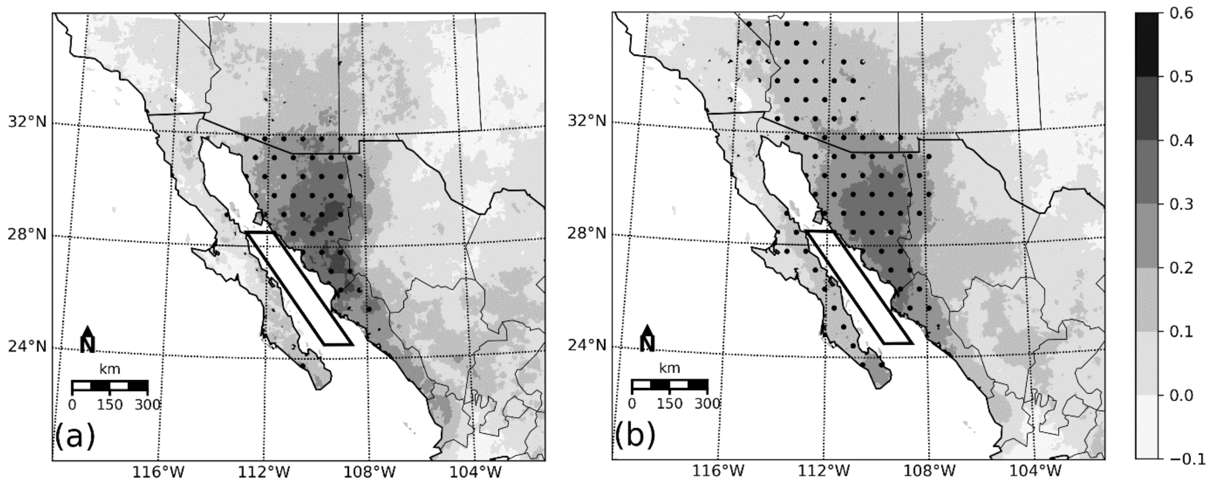

Figure 12. Correlation coefficient between the CFSR daily blh averaged over the black polygon and CHIRPS precipitation for: **(a)** 15 days, and **(b)** 30 days after the monsoon onset from 1982 to 2018. Hatching indicates areas with correlations statistically significant at the 95 % level.

Following Livezey and Chen (1983), we tested the field significance of the correlation patterns to show that the statistically significant results are robust. First, we used the Student's one-tail t-test at $\alpha = 0.05$ to find the percentage of the grid with significant correlations. We found that for the first 15 (30) days of the season, 14.30 % (26.43 %) of the study area passed the t-test. We then performed correlations between the precipitation data and 1000 resampling Monte Carlo bootstrap tests substituting the blh estimates with random numbers at every grid point to determine the areas that correlate with noise. We estimated that the 5% tail of the distribution of areas with "accidental" significant correlations was 6.5 %. Since this value is smaller than the percentages with statistically significant correlations (14.30 % and 26.43 %), we reject the null hypothesis to confirm that they are highly significant and do not occur randomly 93.5 % of the time.

The areas with statistically significant correlations in Fig. 12 are hatched. As can be noted in both plots, all the significant correlations are positive and below 0.6, indicating a moderate, directly proportional relationship between the blh of the GoC and the NAM precipitation. The statistically significant relations (for 15 days, Fig. 12a) are found in northern Sinaloa and the entire state of Sonora. These areas extend northward and include parts of southern Arizona for the 30-day post-onset time frame (Fig. 12b), although the association is more uncertain there according to the correlation coefficients (< 0.2). This is a reasonable outcome if we consider the time window used in the analysis (for larger time windows we would expect higher correlations for this area), the geographic location of Arizona relative to the GoC and the significant contribution of evapotranspiration to NAM precipitation (Dominguez et al., 2008, Hu and Dominguez 2015).

The southern half of the BC peninsula also has a significant relationship in the 30-day window, although much less precipitation occurs over that region and it's probably not directly related with the monsoon itself but rather with the effects of the local breeze flows. These results indicate that the NAM precipitation during the first month of the monsoon season has a clear relation with the GoC boundary layer, further strengthening the hypothesis that the gulf is both a source and a channel for the low-level moisture that fuels the monsoon precipitation.

A positive correlation between rainfall and the GoC surface temperature was conjectured by Erfani and Mitchell, 2014 to be possibly explained, at least in part, by the effects of gulf moisture surges, which are a synoptic feature of the NAM intraseasonal variability characterized by higher pressure, lower temperature, higher moisture and stronger near-surface winds (Stensrud et al., 1997). We have shown that precipitation over Sonora, Sinaloa, and southern Arizona is closely related to the variations of the gulf boundary layer height and that it in turn is related to the GoC SST. The cooler air masses and stronger winds associated to gulf surges likely destabilize the GoC boundary layer and increase its turbulence through greater vertical shear. However, the time scales analyzed in our study do not permit an evaluation of the effects of gulf surges on our hypothesis. Again, more focused research is needed.

4 Summary and Conclusions

In this paper we used rawinsonde and pilot balloon data collected during the 2004 North American Monsoon Experiment (NAME) campaign, as well as satellite and rain-gauge merged precipitation and reanalysis datasets to analyze the temporal and spatial evolution of the Gulf of California (GoC) boundary layer, including the physical mechanisms responsible for its mixing, during the North American Monsoon (NAM) onset phase. Our main findings are:

1. We described the mean vertical profile of the winds observed from seven pilot balloon stations and found that the GoC has a complex breeze regime. During the daytime, onshore flows over both coasts produce convergence over the BC peninsula and divergence over the gulf. At night, the circulation reverses as offshore flows and convergence over the GoC set up. We summarized these results in a new conceptual model for the gulf's local wind systems, centered on the monsoon onset that modifies the one proposed by Badan-Dangon et al. (1991).

2. The daily evolution of the GoC boundary layer height reaches its peak around 1000 LT, and its minima after 2200 LT. This diurnal evolution cycle is closely related to the gulf's breeze regime. The beginning of the nocturnal growth of the boundary layer was observed to be modulated by the presence and intensity of the thermal inversion over the gulf. This nightly development starts earlier before the onset because part of the energy trapped within the boundary layer by the thermal inversion is released as soon as the subsidence over the gulf begins to fade. After the NAM onset, the warming of the sea surface has eroded the thermal inversion and the nocturnal growth of the boundary layer driven by near-surface convergence over the GoC starts at later hours.

3. The average date of the NAM onset between 1982 and 2018 was found to be June 19, which is within the range of previous studies (Xu et al., 2004, Higgins et al., 1999). This date was identified for each season as the first of five consecutive days with CHIRPS daily precipitation averaged over a polygon spanning northern Sinaloa and southern Sonora that exceeded the threshold of 2 mm. The correlation between the onset date and the average monsoon precipitation in the same area is moderate and positive during the first 80 days, and becomes negative afterwards. The highest correlations are found between 20 and 40 days after the onset, indicating that during this time frame, years with an earlier onset were initially drier than those with a later start. This result is in contrast with Higgins et al. (1999) and Douglas and Englehart (1996), possibly because their analysis considered the entire monsoon season.

4. We compared blh estimates from four different reanalysis datasets: CFSR, NARR, MERRA-2 and ERA5. The CFSR reanalysis was found to have the best estimates of the boundary layer height, probably due to its accurate representation of the surface wind field divergence. Still, the horizontal spatial resolution of the CFSR limits its use in the study of the breeze regimes. Therefore, further work with higher spatial resolution data should be considered.

5. We conclude that on interannual timescales there is a strong positive correlation between the GoC SST and its boundary layer height at the time of NAM onset, and in turn, a moderate, directly proportional relationship between the GoC boundary layer height and monsoon precipitation. The regions with higher significant correlations are located over the states of Sinaloa and Sonora during the first days after the onset. Interannual NAM variability is therefore likely to be affected by the ocean processes that govern the GoC seasonal heat balance and numerical climate models with insufficient spatial resolution to adequately resolve the GoC should be interpreted with caution when used to forecast or analyze NAM precipitation.

6. Finally, we examined the sources of turbulence to clarify the processes that mix the GoC boundary layer in the context of the NAM onset. We looked at the non-local static stability and the bulk Richardson Number using 2004 NAME rawinsonde data. According to our findings, the lowest 500 m of the boundary layer become statically unstable after the onset. Also, the mechanical production of turbulence was the most sensitive to the onset, with an increase of over 16 %. Hence, we believe that the turbulence generated by wind shear is the main source for the mixing of the gulf marine layer. The thermal inversion described by Erfani and Mitchell (2014) inhibits the mixing of the boundary layer with the air aloft because the negative buoyancy of the statically stable layer consumes all the mechanical turbulence generated by wind shear before the onset. Once the seasonal warming of the gulf breaks the inversion, mechanical turbulence is no longer consumed and becomes available for mixing.

We have focused this work on explaining how the gulf boundary layer evolves in time and how the vertical mixing occurs during the monsoon onset. The soundings and pilot balloon measurements obtained during the 2004 NAME were the prime data source for this research. Consequently, this study is limited by its temporal coverage and spatial resolution. Future work is planned to include high resolution numerical simulations to conduct a comprehensive analysis of the mixing processes in the boundary layer of the GoC associated with the NAM onset.

Acknowledgments

This work was supported by the National Council of Science and Technology of Mexico (CONACYT Scholarship Grants 486021 and 486022), and CICESE (Internal Grant 621176). The authors thank the SNI-Mexico (15320) for support. The NAME data is accessible from the NCAR/EOL website. All the other data used in this study (CFSR, NARR, MERRA-2, ERA5, NOAA-OI and CHIRPS) are also available from their websites. We are very grateful to Bob Dattore for his support with the CFSR dataset. We extend our thanks to Fco. Javier Ponce I. for his help drawing two sketches. We also appreciate the comments from the anonymous reviewers.

References

Adams, D. K., and A. C. Comrie (1997), The north American monsoon. *Bull. Amer. Meteor. Soc*., **78**, 2197-2214, https://doi.org/10.1175/1520-0477(1997)078%3C2197:TNAM%3E2.0.CO;2.

Arya, P. S. (2001), *Introduction to Micrometeorology*. Academic Press, Volume 79 of International Geophysics, ISSN 0074-6142, 420 pp.

Badan-Dangon, A., Dorman, C. E., Merrifield, M. A., and C. D. Winant (1991), The lower atmosphere over the Gulf of California. *J. Geophys. Res. Oceans*., **96**, 16877-16896, https://doi.org/10.1029/91JC01433.

Barron, J. A., Metcalfe, S. E., and J. A. Addison (2012), Response of the North American monsoon to regional changes in ocean surface temperature. *Paleoceanography*., **27**, PA3206, https://doi.org/10.1029/2011PA002235.

Castro, R., M.F Lavín and P. Ripa (1994), Seasonal heat balance in the Gulf of California. *J. Geophys. Res. Oceans*., **99**, 3249-3261, https://doi.org/10.1029/93JC02861

Cavazos T, Luna-Niño R, Cereza-Mota R, Fuentes-Franco R, Méndez M, Pineda Martínez LF, and E. Valenzuela (2019), Intercomparison of regional climate models and climatic trends in the CORDEX-CAM (Central America, Caribbean and Mexico) domain. *Int. J. Climatol*., **2019**, 1-25, https://doi.org/10.1002/joc.6276

Ciesielski, P. E., and R. H. Johnson (2008), Diurnal cycle of surface flows during 2004 NAME and comparison to model reanalysis. *J. Climate*., **21**, 3890-3913, https://doi.org/10.1175/2008JCLI2206.1.

Dee, D. P. and Coauthors (2011), The ERA-Interim reanalysis: Configuration and performance of the data assimilation system. *Q. J. Royal Meteorol. Soc*., **137**, 553-597, https://doi.org/10.1002/qj.828.

Dominguez, F., Miguez-Macho, G., and H. Hu (2016), WRF with Water Vapor Tracers: A Study of Moisture Sources for the North American Monsoon. *J. Hydrometeorol*., **17**, 1915-1927, https://doi.org/10.1175/JHM-D-15-0221.1.

Dominguez, F., P. Kumar and E. R. Vivoni (2008), Precipitation recycling variability and ecoclimatological stability—A study using NARR data. Part II: North American monsoon region. *J. Climate*., **21**, 5187–5203, https://doi.org/10.1175/2008JCLI1760.1.

Douglas, M.W., Maddox, R.A., Howard, K., and Reyes, S (1993), The mexican monsoon. *J. Climate.*, **6(8)**, 1665-1677, https://doi.org/10.1175/1520-0442(1993)006%3C1665:TMM%3E2.0.CO;2

Douglas, A. V., and P. J. Englehart (1996), An analysis of the starting date for the summer monsoon in western Mexico and southeast Arizona. *Proc. 20th Annual Climate Diagnostics and Prediction Workshop*., 207–211.

Erfani, E., and D. Mitchell (2014), A partial mechanistic understanding of the North American monsoon. *J. Geophys. Res.Atmos*., **119**, 13-096, https://doi.org/10.1002/2014JD022038.

Farr, T.G. and Coauthors (2007), The shuttle radar topography mission. *Rev. Geophys*., **45**, RG2004, https://doi.org/10.1029/2005RG000183.

Funk, C., and Coauthors (2015), The climate hazards infrared precipitation with stations—a new environmental record for monitoring extremes. *Sci. Data*., **2**, 150066, https://doi.org/10.1038/sdata.2015.66.

Gelaro, R., and Coauthors (2017), The Modern-Era Retrospective Analysis for Research and Applications, Version 2 (MERRA-2). *J. Climate*., **30**, 5419–5454, https://doi.org/10.1175/JCLI-D-16-0758.1.

Gochis, D. J., and Coauthors (2007), Northwest Mexico NAME Event Raingage Network (NERN) Daily Data. Version 1.0. https://doi.org/10.26023/PZEM-AQH9-390E. Accessed 24 Jun 2019.

Gómez-Valdivia, F., A. Parés-Sierra and A.L. Flores-Morales (2015), The Mexican Coastal Current: A subsurface seasonal bridge that connects the tropical and subtropical Northeastern Pacific. Cont. Shelf Res., **110**, 100-107, https://doi.org/10.1016/j.csr.2015.10.010

Gutzler, D. S (2004), An index of interannual precipitation variability in the core of the North American monsoon region. *J. Climate*., **17**, 4473-4480, https://doi.org/10.1175/3226.1.

Higgins, R. W., and Coauthors (2006), The NAME 2004 Field Campaign and Modeling Strategy. *Bull. Amer. Meteor. Soc*., **87**, 79-94, https://doi.org/10.1175/BAMS-87-1-79.

Higgins, R. W., Chen, Y., and A. V. Douglas (1999), Interannual variability of the North American warm season precipitation regime. *J. Climate*., **12**, 653-680, https://doi.org/10.1175/1520-0442(1999)012%3C0653:IVOTNA%3E2.0.CO;2

Hu, H., and F. Dominguez (2015), Evaluation of oceanic and terrestrial sources of moisture for the North American monsoon using numerical models and precipitation stable isotopes. *J. Hydrometeor*., **16**, 19–35, https://doi.org/10.1175/JHM-D-14-0073.1.

Johnson, R. H., Ciesielski, P. E., L'Ecuyer, T. S., and A. J. Newman (2010), Diurnal cycle of convection during the 2004 North American Monsoon Experiment. *J. Climate*., **23**, 1060-1078, https://doi.org/10.1175/2009JCLI3275.1.

Liu, S., and X. Z. Liang (2010), Observed Diurnal Cycle Climatology of Planetary Boundary Layer Height. *J. Climate*., **23**, 5790-5809, https://doi.org/10.1175/2010JCLI3552.1.

Livezey, R. E., and W. Y. Chen (1983), Statistical field significance and its determination by Monte Carlo techniques. *Mon. Weather. Rev*., **11**, 46-59, https://doi.org/10.1175/1520-0493(1983)111%3C0046:SFSAID%3E2.0.CO;2.

Mesinger, F. and Coauthors (2006), North American regional reanalysis. *Bull. Am. Meteorol. Soc*., **87**, 343-360, https://doi.org/10.1175/BAMS-87-3-343.

Mitchell, D. L., D. C. Ivanova, R. Rabin, T. J. Brown, and K. Redmond (2002), Gulf of California sea surface temperatures and the North American monsoon: Mechanistic implications from observations, *J. Clim.*, **15**, 2261–2281, https://doi.org/10.1175/1520-0442(2002)015<2261:GOCSST>2.0.CO;2

Reynolds, et al., (2007), Daily High-Resolution-Blended Analyses for Sea Surface Temperature, *J. Clim*., **20**, 5473-5496, https://doi.org/10.1175/2007JCLI1824.1

Saha, S., and Coauthors (2010), The NCEP climate forecast system reanalysis. *Bull. Amer. Meteor. Soc*., **91**, 1015-1058, https://doi.org/10.1175/2010BAMS3001.1.

Seidel, D.J, Chi O. Ao, and Kun Li (2010), Estimating climatological planetary boundary layer heights from radiosonde observations: Comparison of methods and uncertainty analysis. *J. Geophys. Res*., **115**, D16113, https://doi.org/10.1029/2009JD013680.

Stensrud, D. J., R. L. Gail, and M. K. Nordquist (1997), Surges over the Gulf of California during the Mexican monsoon. *Mon. Weather Rev*., **125**, 417–437, https://doi.org/10.1175/1520-0493(1997)125<0417:SOTGOC>2.0.CO;2.

Stull, R. B. (2012), *An introduction to boundary layer meteorology*. Springer Science & Business Media, 670 pp.

Turrent, C., and O. Zaitsev (2014), Seasonal cycle of the near-surface diurnal wind field over the bay of La Paz, Mexico. *Bound-Lay. Meteorol*., **151**, 353-371, https://doi.org/10.1007/s10546-014-9908-4.

Turrent, C., and T. Cavazos (2009), Role of the land-sea thermal contrast in the interannual modulation of the North American Monsoon. *Geophys. Res. Lett*., **36**, L02808, https://doi.org/10.1029/2008GL036299.

Wallace, J. M. and P. V. Hobbs (2006), *Atmospheric science: An introductory survey*. Elsevier, 504 pp.

Wang, X. Y., and K. C. Wang (2014), Estimation of atmospheric mixing layer height from radiosonde data. *Atmos. Meas. Tech*., **7**, 1701-1709, https://doi.org/10.5194/amt-7-1701-2014.

Xu, J., Gao, X., Shuttleworth, J., Sorooshian, S., and E. Small (2004), Model climatology of the North American monsoon onset period during 1980–2001. *J. Climate*., **17**, 3892-3906, https://doi.org/10.1175/1520-0442(2004)017%3C3892:MCOTNA%3E2.0.CO;2.

Zuidema, P., C. Fairall, L. M. Hartten, J. E. Hare, and D. Wolfe (2007), On Air–Sea Interaction at the Mouth of the Gulf of California. *J. Climate*., **20**, 1649–1661, https://doi.org/10.1175/JCLI4089.1.